Draft version November 20, 2014
Preprint typeset using LaTeX style emulateapj v. 04/17/13

arXiv:1411.5020v1 [astro-ph.GA] 18 Nov 2014

SMT CO (2-1) OBSERVATIONS OF NEARBY STAR-FORMING GALAXIES

Xue-Jian Jiang (蒋雪健)[1,2,3,4], Zhong Wang[2], Qiusheng Gu[1,3,4], Junzhi Wang[5] and Zhi-Yu Zhang[6,7]

Draft version November 20, 2014

ABSTRACT

We present CO J=2-1 observations towards 32 nearby gas-rich star-forming galaxies selected from the ALFALFA and WISE catalogs, using the Sub-millimeter Telescope[a]. Our sample is selected to be dominated by intermediate-M_* galaxies. The scaling-relations between molecular gas, atomic gas and galactic properties (stellar mass, NUV$-r$ and *WISE* color W3$-$W2) are examined and discussed. Our results show that (1). In the galaxies with stellar mass $M_* \leqslant 10^{10}\ M_\odot$, H I fraction ($f_{\rm HI} \equiv M_{\rm H\,I}/M_*$) is significantly higher than that of more massive galaxies, while H_2 gas fraction ($f_{\rm H_2} \equiv M_{\rm H_2}/M_*$) remain nearly unchanged. (2). Comparing with $f_{\rm H_2}$, $f_{\rm HI}$ correlates better with both M_* and NUV$-r$. (3). A new parameter, *WISE* color W3$-$W2 (12 μm$-$4.6 μm) is introduced, which is similar to NUV$-r$ in tracing star formation activity, and we find that W3$-$W2 has a tighter anti-correlation with log $f_{\rm H_2}$ than the anti-correlation of (NUV$-r$) - $f_{\rm HI}$, (NUV$-r$) - $f_{\rm H_2}$ and (W3$-$W2) - $f_{\rm HI}$. This indicates that W3$-$W2 can trace the H_2 fraction in galaxies. For gas ratio $M_{\rm H_2}/M_{\rm H\,I}$, only in the intermediate-M_* galaxies it appears to depend on M_* and NUV$-r$. We find a tight correlation between the molecular gas mass $M_{\rm H_2}$ and 12 μm (W3) luminosities ($L_{12\,\mu{\rm m}}$), and the slope is close to unity (1.03 ± 0.06) for the SMT sample. This correlation may reflect that the cold gas and dust are well mixed on global galactic scale. Using the all-sky 12 μm (W3) data available in *WISE*, this correlation can be used to estimate CO flux for molecular gas observations and can even predict H_2 mass for star-forming galaxies.

Keywords: galaxies: evolution; galaxies: ISM; infrared: galaxies; ISM: molecules; radio lines: galaxies

1. INTRODUCTION

In all star forming systems from Galactic molecular clouds to high redshift galaxies, cold atomic and molecular gases (H I and H_2) are the raw material that form stars and drives the evolution of galaxies. Understanding of the relationships between cold gas and global properties of galaxies, such as star formation activities, has been greatly improved thanks to the recent multi-wavelength advances. For example, galaxies show strongly bimodal distributions in their integrated colors, which indicates two modes in the galaxy evolution histories, that young galaxies with active star-formation in the "blue cloud", appeared to rapidly evolve into the "red sequence" populated by quiescent galaxies with little star-formation (Kennicutt & Evans 2012). This transition must be preceded by the transformation from H I to H_2, the assembly of molecular clouds, and star-formation therein (Krumholz 2013; Schruba et al. 2011).

Email: xjjiang@nju.edu.cn
[1] School of Astronomy and Space Science, Nanjing University, Nanjing 210093, China
[2] Harvard-Smithsonian Center for Astrophysics, MS 66, 60 Garden St., Cambridge, MA 02138, United States
[3] Key Laboratory of Modern Astronomy and Astrophysics, Nanjing University, Ministry of Education, Nanjing 210093, China
[4] Collaborative Innovation Center of Modern Astronomy and Space Exploration, Nanjing 210093, China
[5] Shanghai Astronomical Observatory, Chinese Academy of Sciences, 80 Nandan Road, Shanghai 200030, China
[6] The UK Astronomy Technology Centre, Royal Observatory Edinburgh, Blackford Hill, Edinburgh, EH9 3HJ, United Kindom
[7] ESO, Karl Schwarzschild Strasse 2, D-85748 Garching, Munich, Germany
[a] The SMT is operated by the Arizona Radio Observatory (ARO), Steward Observatory, University of Arizona.

Star forming galaxies were found to fall on a main sequence (MS) in the relation between stellar mass and star formation rate (Daddi et al. 2007), and recent studies found that the scatter in the MS is remarkably small at different redshifts, implying that the majority of star forming galaxies are 'normal' galaxies lying along the relation (Guo et al. 2013; Rodighiero et al. 2011). Particularly, intermediate-mass (or low mass) galaxies ($M_* < 10^{10} M_\odot$) are still not well understood. Their number dominates the galaxy populations, many of them are cold ISM dominated and have lower metallicities than solar value. As a result their star formation properties are distinct from massive galaxies. Low mass galaxies were found to be more gas rich and inefficient in transforming their gas into stars (Blanton & Moustakas 2009), but they may dominate the present star-forming galaxy populations rather than massive galaxies (downsizing effect), and may help understand high-z galaxies since the physical conditions in low mass systems such as high gas ratio and low metallicity resemble those at the early universe.

Recent studies have found a steep decline of cosmic star formation rate density between $z = 1$ and 0, and peaks at $z \sim 1 - 2$ (Bouwens et al. 2011; Carilli & Walter 2013), and this evolution appears to be strongly regulated by the evolution of cold gas content, of which the most important parameters are gas fraction $f_{\rm gas}$ ($M_{\rm H_2}/M_*$ and $M_{\rm H\,I}/M_*$, sometimes $M_{\rm gas}/(M_* + M_{\rm gas})$) and gas phase ratio $r_{\rm gas}$ ($M_{\rm H_2}/M_{\rm H\,I}$). $f_{\rm gas}$ and $r_{\rm gas}$ have been found to be significantly increased toward high redshift, and the pronounced evolution of $f_{\rm gas}$ seems to resemble the evolution of SFR (Combes et al. 2013), implies its important role in determining the star formation history. Moreover, Tacconi et al. (2013) shows a trend of increas-

ing $f_{\rm gas}$ with decreasing stellar mass (see also Saintonge et al. 2011a), implying that the cosmic gas density could be higher than current derived values (Carilli & Walter 2013). Although representing main-sequence star-forming galaxies, the sample by Tacconi et al. (2013) were limited to the high-mass end of galaxies distribution, and studies on low- to intermediate-stellar mass galaxies would provide crucial constraint on the cosmic gas content as well as star-formation history. In this context, the study of nearby galaxies of intermediate-stellar mass can provide a benchmark of high-z studies. In existing CO surveys, galaxies beyond our immediate vicinity are almost entirely dominated by massive systems (COLD GASS, Saintonge et al. 2011a) and/or Luminous Infrared Galaxies (LIRGs, Genzel et al. 2010), while surveys of intermediate–mass galaxies were limited by distance (HERACLES, Leroy et al. 2009) or environment (AMIGA, Lisenfeld et al. 2011). This stands in sharp contrast to surveys of other wavelengths (e.g., SDSS in optical or GALEX in UV), where homogeneous samples of ordinary (and many low–mass) galaxies out to hundreds of Mpc distance are available.

Atomic gas (neutral hydrogen) is traced by H I 21-cm hyperfine transition line (Haynes et al. 2011) and molecular gas (mainly H_2) mass can be traced by carbon monoxide, typically ^{12}CO(J=1→0) (Young & Scoville 1991; Saintonge et al. 2011a; Lisenfeld et al. 2011) and ^{12}CO(J=2→1) (Leroy et al. 2013). Surveys towards very nearby galaxies such as SINGS (Kennicutt et al. 2003) and THINGS (Walter et al. 2008) have conducted detailed analysis for spiral disk of galaxies, while there are also surveys with larger sample of greater distances ($>$ 100 Mpc, e.g., the COLD GASS, Saintonge et al. 2011a,b), that mainly focus on the global scaling relations. Much recent effort has been devoted to study of the correlation between molecular gas tracers (CO, HCN, HCO^+ and CS etc.) and star formation in nearby galaxies, both individually and as a function of Hubble type (Zhang et al. 2014; Gao & Solomon 2004; Calzetti et al. 2007; Kennicutt et al. 2009; Bigiel et al. 2011). On global scales ($\gtrsim$ 1 kpc) H I and H_2 appear to depend on other galactic physical properties, and such scaling-relations can help better understand the role of cold gas in the histories of galaxy evolution and star formation.

The Arecibo ALFALFA survey (α.40, Giovanelli et al. 2005) scanned a large area of the sky and aimed to study the H I content of normal galaxies out to $\sim$ 250 Mpc (Haynes et al. 2011). It so far covers $\sim$ 3,000 square degrees of the sky and contains more than 15,000 galaxies, and is characterized by a maximum overlap with the coverage of both the SDSS and GALEX. Comparing with optical-selected sample, this H I-selected sample represents a less evolved galaxy population, in which a transition in star formation properties is found at around $M_* \sim 10^{9.5} M_\odot$. Below this mass, galactic star formation is found to be strongly regulated by H I mass rather than stellar mass (Huang et al. 2012). Thus a survey of molecular gas in the intermediate-mass galaxies selected from the ALFALFA sample would provide a key missing link between star formation and global gas content (H_2 + H I) in these galaxies.

In this paper, we describe our SMT sample in Section 2. The SMT observation and results are presented in Section 3. We present our calculations of molecular gas mass for the SMT sample in Section 3.1, as well as the stellar mass calculations for both the SMT sample and the AMIGA sample. The main results are presented in section 4. In section 4.1 the different samples are compared, in sections 4.2 and 4.3 we discuss the scaling relations of gas fraction ($M_{\rm gas}/M_*$) and gas ratio ($M_{\rm H_2}/M_{\rm H\,I}$), and in Section 4.4 the correlation between molecular gas and *WISE* infrared properties is discussed. Throughout this work, we assume the cosmological parameters ($\Omega_{\rm m} = 0.3, \Omega_\Lambda = 0.7, H_0 = 70$) which are consistent with the *Wilkinson Microwave Anisotropy Probe* Third Year results in combination with other data (Spergel et al. 2007).

2. THE SAMPLE

2.1. *The SMT sample*

To obtain a representative sample of nearby galaxies selected based on gas content and to explore their infrared properties, we begin from the most up-to-date ALFALFA survey catalog and look for counterparts in the *WISE* all-sky catalog to construct the parent sample. Comparing with optical-selected samples, the ALFLAFA is an H I-selected sample thus represents a less evolved galaxy population.

The Wide-field Infrared Survey Explorer (*WISE*, Wright et al. 2010) Catalog provide all-sky image data in four infrared bands (3.4, 4.6, 12 and 22 μm), with an angular resolution of 6.1″, 6.4″, 6.5″ and 12.0″, respectively. *WISE* achieved 5σ point source sensitivities better than 0.08, 0.11, 1 and 6 mJy, respectively, in unconfused regions on the ecliptic in the four bands.

First, we cross–matched the ALFALFA α.40 catalog with the *WISE* all-sky catalog, and selected galaxies based on the following criteria: (1) S/N $\geqslant$ 5 for the W1 (3.4 μm), W2 (4.6 μm) and W3 (12 μm) bands of *WISE*, and S/N $\geqslant$ 3 for W4 (22 μm). Because W4 is much less sensitive than other bands, and we are not using W4 in our analysis, so we lower the requirement for the W4 band; (2) An object is defined as being the same one in both catalogs if the difference between its coordinates in *WISE* catalog and ALFALFA catalog is $\leqslant$ 3″. We obtained 5434 ALFALFA–*WISE* counterparts as a parent sample.

Second, based on this parent sample, we limited the distance of the sample to be in the range of 20–165 Mpc, and required that galaxies are covered by the GALEX MIS (Medium Image Survey, exposure time $>$ 1500s).

Third, we selected infrared bright (W3 $\leqslant$ 10 and W4 $\leqslant$ 8) galaxies to assure a high detection probability within realistic integration time. The stellar masses of the sample, which were obtained from the MPA-JHU catalog[1], are then selected to be distributed in the range of $10^8 - 10^{11}$ $M_\odot$. Therefore we got 115 galaxies as candidates for the observation. For these galaxies, we visually checked the optical images of these galaxies from SDSS to exclude those obvious interacting or merger systems, to assure that the SMT telescope only obtain CO emission from the target galaxies. we used the W3 magnitude and H I linewidth to estimate the CO flux of the sample, and observed those relatively strong sources.

[1] http://www.mpa-garching.mpg.de/SDSS/

30 galaxies were selected from this ALFALFA–*WISE* parent sample, and other two LIRGs (Luminous Infrared Bright Galaxies) were added for comparison. Hence there are 32 galaxies in the final SMT sample. Although the selection might biases the sample to gas-rich and/or infrared bright galaxies, these galaxies still span a range in a set of more fundamental parameters, such as $M_{\rm H_2}$, $M_{\rm H\,I}$ and M_*, and most of them have stellar masses $< 10^{10} M_\odot$, so that this sample can still fulfill our goal that focus on intermediate-M_* galaxies. We list the general information of the SMT sample in Table 1.

2.2. *Literature CO 1-0 data*

Since there were a few molecular gas surveys conducted recently, we combined our SMT sample which was selected from the ALFLAFA-*WISE* parent sample, with these surveys, so that we can compare the properties and/or relations of different galaxies.

COLD GASS (CO Legacy Database for the GASS, Saintonge et al. 2011a; Catinella et al. 2012) is a molecular gas survey in nearby massive ($M_* \geqslant 10^{10} M_\odot$) galaxies. By measuring CO 1-0 with the IRAM 30-m telescope, they have provided $M_{\rm H_2}$ for 366 galaxies, 194 of which were treated as secure CO 1-0 detection (S/N $\geqslant$ 5).

AMIGA (Analysis of the interstellar Medium of Isolated GAlaxies) is another galaxy survey in nearby isolated galaxies, which aimed to address the environmental effects on cold gas content of galaxies. Lisenfeld et al. (2011) has provided CO 1-0, $M_{\rm H_2}$ as well as $M_{\rm H\,I}$ data for 273 AMIGA galaxies, of which 180 were from observations from IRAM 30-m, FCRAO 14-m (Five College Radio Astronomical Observatory) and the rest from other literature.

We searched in the *WISE* all-sky catalog for counterparts of the COLD GASS and AMIGA-CO sample. There are *WISE* counterparts for 349 COLD GASS galaxies, and 179 AMIGA-CO galaxies, respectively. Among these counterparts, 183 COLD GASS sources have S/N $\geqslant$ 5 in the W1, W2, W3 bands as well as CO detection, and 86 AMIGA-CO sources satisfied the same criteria. In our discussion of the relationship between *WISE* infrared emission and molecular gas, we only use these high S/N sample. When exploring the relation between CO emission and *WISE* infrared emission, we found a tight correlation between the CO and 12 μm emission for both COLD GASS and AMIGA survey (we will discuss this relation in detail in Sec. 4.4). With these combined sample, we can therefore investigate the scaling-relations in intermediate-M_* galaxies, and avoid the possible environmental effect induced in the AMIGA-CO sample.

2.3. *SDSS and GALEX data*

In order to construct a multi-wavelength dataset for comprehensive analysis and comparison with the COLD GASS and AMIGA–CO, We have collected SDSS and *GALEX* data for both the SMT sample and the AMIGA–CO sample.

The newest data release of Sloan Digital Sky Survey, SDSS–III DR9 (hereafter DR9), have provided more available images and photometric measurements in *ugriz* bands. We run query with our SMT sample and the AMIGA–CO sample in DR9, and obtained photometric magnitudes (*ugriz*, extinction corrected) and morphological parameters (R90 and R50) for 30 SMT galaxies and 186 AMIGA–CO galaxies. Since extended sources are probably "deblended" in the SDSS photometry process (Huang et al. 2012), we check the SDSS flags for each galaxy to make sure that they are the "brightest child" photometric object extracted from the galaxy.

However, one SMT galaxy, AGCNr 4584, has an abnormal z-band magnitudes in DR9 ($z_{\rm dr9} = 22.9^{\rm mag}$), which significantly deviates from its value in DR7 ($z_{\rm dr7} = 13.1^{\rm mag}$) as well as other galaxies' z-band magnitudes, which are all brighter than $16^{\rm mag}$. After inspecting the SDSS images of AGCNr 4584, we found that the photometric position of this galaxies has been shifted in DR9 (and DR8) but is not in the galactic nucleus, which may be the reason of the abnormal photometry. Thus for AGCNr 4584, we adopt its data from DR7 instead of DR9.

We also searched in the *GALEX* GR6/7 catalog and found *GALEX* counterparts for 27 SMT galaxies and 223 AMIGA-CO galaxies. For the AMIGA-CO sample, 9% SDSS counterparts and 28% *GALEX* counterparts have angular separation larger than 3″, but we did visual inspection and assure that they are the genuine counterparts and are not contaminated by nearby galaxies. In fact, since the AMIGA sample are all isolated galaxies, mismatch and/or contamination is not likely for nearly all the AMIGA-CO galaxies. The NUV magnitudes is corrected for Galactic extinction following Wyder et al. (2007).

3. SMT OBSERVATION AND DATA REDUCTION

The SMT observations were carried out in December, 2012. We spent 59 hours in total, including $\sim 40\%$ overhead, to observe CO 2-1 ($\nu_{\rm rest} = 230.538$ GHz) towards 32 galaxies. We used the Forbes Filter Bank system, which provide 1 MHz per channel and 1024 channels in total, corresponding to a velocity coverage of 1300 km s^{-1} bandwidth for each polarization. During the observations the typical system temperature was less than 300 K. Each galaxy was integrated until CO 2-1 was detected or three hours integration time was reached. Beam Switch mode with 2′ throw were used and pointing and focus were checked every 1.5 hours using DR 21. Saturn was used for flux calibration. The HPBW (half-power beamwidth) of the SMT at this frequency is about 33″.

The data were reduced with the `class` program of the `gildas` package[2]. Poor scans and bad channels were flagged, and a three degree polynomial baseline was fitted to subtract the unstable baseline from each spectrum. The root-mean-square (RMS) noise level of each averaged spectrum of the sample target was obtained at a velocity resolution of 11 to 21 km s^{-1}, based on the linewidth of each galaxy.

The velocity-integrated intensities of CO 2-1 are calculated using

$$I = \int_{\Delta V} T_{\rm mb} {\rm d}v, \tag{1}$$

where $T_{\rm mb}$ is the main beam brightness temperature, and ΔV is the velocity range used to integrate the inten-

[2] `http://iram.fr/IRAMFR/GILDAS/`

Table 1
General data of the SMT sample

galaxy	RA (J2000) Dec		Distance	log $M_{\rm HI}$[a]	r_{50}[b]
	[h m s]	[° ′ ″]	[Mpc]	[$M_\odot$]	[″]
AGC 230	00:23:59.4	+15:46:14	74.8	10.2	11.5
AGC 233	00:24:42.8	+14:49:28	74.3	9.7	6.5
AGC 463	00:43:32.4	+14:20:33	62.1	9.7	16.8
AGC 978	01:25:13.2	+14:52:20	86.6	9.9	11.6
AGC 629	02:08:25.0	+14:20:57	60.6	10.0	9.4
AGC 456	08:32:03.5	+24:00:37	79.8	10.0	14.6
AGC 473	08:33:56.7	+26:58:20	51.9	9.7	8.2
AGC 584	08:45:59.5	+12:37:11	61.3	9.9	16.3
AGC 760	09:04:54.2	+25:00:12	44.7	9.1	12.2
AGC 823	09:10:41.8	+07:12:23	23.8	9.1	7.6
AGC 122	14:15:23.8	+04:24:28	86.2	9.8	7.5
AGC 172	14:20:04.4	+03:59:32	27.8	9.1	15.6
AGC 9346	14:31:57.4	+06:15:00	36.3	9.8	12.1
AGC 9696	15:05:30.5	+08:31:26	121.5	10.0	6.7
AGC 10384	16:26:46.6	+11:34:49	74.4	10.1	7.4
AGC 12481	23:17:36.6	+14:00:02	63.4	9.8	6.5
AGC 12586	23:24:49.3	+15:16:31	61.2	9.8	11.1
AGC 101985	00:20:48.6	+14:13:28	75.5	9.0	2.0
AGC 110202	01:19:32.9	+14:52:19	56.4	9.1	5.4
AGC 171860	07:49:56.0	+26:02:13	70.8	9.2	5.5
AGC 180293	08:28:22.3	+25:07:29	32.8	8.4	9.2
AGC 180931	08:07:10.3	+24:23:21	157.8	9.2	7.2
AGC 180945	08:09:45.5	+25:52:50	110.7	9.8	5.5
AGC 240580	14:40:22.7	+09:28:34	124.0	9.2	7.0
AGC 241492	14:20:42.2	+05:29:08	120.7	10.4	4.4
AGC 241716	14:55:21.0	+05:17:52	95.2	9.7	6.4
AGC 242440	14:08:46.8	+04:54:35	76.9	9.6	1.9
AGC 250019	15:03:30.7	+10:49:47	147.9	9.5	4.1
AGC 330149	23:14:59.5	+14:59:19	165.0	9.8	9.6
AGC 721352	09:07:08.3	+25:20:32	41.8	8.5	7.8
PGC 003183	00:54:03.6	+73:05:12	68.0	9.9	...
UGC 11898	22:04:36.1	+42:19:38	61.9	9.0	...

Note: [a] $M_{\rm H\,I}$ are from the ALFALFA α.40 catalog.
[b] Half-light radius r_{50} in unit of arcsec, containing 50% of the r band flux.

Table 2
Estimated data of the SMT sample

galaxy	RMS[a]	FWHM	$I_{\rm CO}$	log $M_{\rm H_2}$	log M_*
	[mK]	[km s^{-1}]	[K km s^{-1}]	[$M_\odot$]	[$M_\odot$]
AGC 230	1.6	104.2	1.20±0.09	9.08	9.88
AGC 233	1.4	105.7	0.85±0.10	8.92	9.76
AGC 463	2.5	168.8	7.09±0.18	9.69	10.42
AGC 978	0.9	125.0	0.43±0.05	8.79	9.95
AGC 629	0.9	311.6	4.98±0.07	9.53	10.33
AGC 456	1.3	63.4	0.86±0.06	8.96	10.15
AGC 473	1.8	42.6	0.28±0.04	8.09	9.37
AGC 584	2.6	53.2	1.52±0.08	8.96	9.56
AGC 760	1.0	147.1	1.46±0.07	8.66	9.72
AGC 823	1.2	62.8	0.47±0.06	7.53	8.28
AGC 122	2.2	31.6	0.52±0.06	8.79	9.49
AGC 172	2.0	163.8	2.68±0.16	8.46	9.66
AGC 9346	2.0	187.5	1.61±0.15	8.49	9.28
AGC 9696	2.7	85.2	1.86±0.13	9.65	10.62
AGC 10384	1.8	359.4	4.64±0.20	9.60	9.98
AGC 12481	3.3	57.6	2.54±0.16	9.24	9.23
AGC 12586	1.6	116.0	2.85±0.13	9.26	10.49
AGC 101985	1.0	46.4	0.16±0.04	8.19	9.06
AGC 110202	1.1	63.2	0.30±0.06	8.25	9.10
AGC 171860	1.1	42.1	< 0.09	<7.89	9.00
AGC 180293	1.7	42.0	0.86±0.07	8.15	9.10
AGC 180931	1.3	16.0	0.11±0.03	8.67	10.40
AGC 180945	0.9	63.7	0.23±0.04	8.66	9.13
AGC 240580	1.7	106.6	0.48±0.09	9.08	9.78
AGC 241492	0.8	106.5	0.52±0.03	9.08	9.93
AGC 241716	3.1	21.6	0.44±0.07	8.81	9.64
AGC 242440	2.5	32.2	0.21±0.06	8.31	8.75
AGC 250019	1.2	97.1	0.31±0.05	9.06	9.50
AGC 330149	1.8	32.6	0.54±0.05	9.44	10.37
AGC 721352	1.3	63.0	1.13±0.07	8.48	9.40
PGC 003183	2.5	105.5	19.96±0.23	10.19	...
UGC 11898	2.5	242.6	7.79±0.23	9.70	...

Note: This table list the measurements of CO 2-1 spectra, including noise level, line width, line integrated intensity, $M_{\rm H_2}$ and M_*.
[a] RMS noise level of the smoothed spectra.

sity. Molecular line intensity in antenna temperature T_a^* is converted to main beam temperature $T_{\rm mb}$ using $T_{\rm mb} = \eta_{\rm eff} T_a^*$, where the efficiency factor $\eta_{\rm eff} = F_{\rm eff}/B_{\rm eff} = 77\%$ ($F_{\rm eff}$: forward efficiency; $B_{\rm eff}$: Beam efficiency) was measured in the flux calibration. The peak $T_{\rm mb}$ of the sample are in the range between about 3 and 80 mK. The basic measured results of the SMT sample, including their RMS, linewidth and integrated intensities, are listed in Table 2.

The CO 2-1 Spectra of the 32 galaxies obtained by the SMT are shown in Figure. 7 in the Appendix. Only one galaxy AGCNr 171860 was a non-detection, and the 3σ upper limits of its CO integrated intensity and $M_{\rm H_2}$ are derived, with its ΔV in equation (1) set to the H I linewidth (W_{50}) from the ALFALFA catalog. Table 2 also list the calculated $M_{\rm H_2}$ and M_* of the sample, and some technical details are discussed in the following sections. In Figure. 7 the radial velocities were normalized to that of their H I velocities from ALFALFA (V_{helio}), and nearly all the CO 2-1 velocities are consistent with their H I velocities, except for a few that have low S/N (AGCNr 978, 101985, 241492, 242440). It is unlikely that the H_2 and H I are spatially inconsistent, instead we suggest that such offset between $V_{\rm HI}$ and $V_{\rm CO}$ are at least partially resulted from the observational uncertainties.

Figure. 7 also shows that, for some SMT galaxies, especially those have large line widths, their CO 2-1 spectra exhibit some structures, such as offset peaks and/or multiple peaks (e.g., AGCNr 463, 1629, 9172, 10384). Although we do not have spatially-resolved CO images for these galaxies, their spectra do reflect the clumpy distribution of $M_{\rm H_2}$ in late type galaxies, and the offset CO peaks suggest that $M_{\rm H_2}$ may locate in circumnuclear regions and/or spiral arms in the form of giant molecular clouds, which is consistent with that reveal by imaging surveys (e.g., Rahman et al. 2012).

3.1. *Calculation of $M_{\rm H_2}$ and M_**

The total molecular gas of a galaxy is computed using $M_{\rm H_2} = \alpha_{\rm CO} L'_{\rm CO}$, and the CO line luminosity is calculated following Solomon et al. (1997):

$$L'_{\rm CO} = 3.25 \times 10^7 S_{\rm CO} \Delta V \nu_{\rm obs}^{-2} D_L^2 (1+z)^{-3} \qquad (2)$$

where CO line intensity $S_{\rm CO}\Delta V$ in units of Jy km s^{-1}, observing frequency $\nu_{\rm obs}$ in GHz, luminosity Distance D_L in Mpc, and $L'_{\rm CO}$ in K km s^{-1} pc^2.

We adopt a CO 2-1/CO 1-0 line ratio (R21) of 0.7, and a CO(1-0)-to-H_2 conversion factor $\alpha_{\rm CO} = 4.35\ M_\odot ({\rm K\,km\,s^{-1}\,pc^2})^{-1}$, equivalent to $X_{\rm CO} = 2 \times 10^{20}$ cm^{-2}(K km s^{-1})$^{-1}$, which are consistent with that used in COLD GASS and AMIGA-CO, as well as recent studies of resolved star-forming regions in nearby galaxies (Leroy et al. 2013). For more detail about R21 and $\alpha_{\rm CO}$

in nearby galaxies, we refer the readers to Leroy et al. (2013) and Sandstrom et al. (2013). All the molecular gas masses in this paper include a factor of 1.36 correcting for the presence of heavy elements (mostly helium). Although the $M_{\rm H_2}$ could not be directly compared with that derived from CO 1-0, the HERACLES survey (Leroy et al. 2013; Sandstrom et al. 2013) have demonstrated that CO 2-1 is able to robustly trace global molecular gas.

The mean error brought by the line measurements itself is about 10%, and other error sources including calibration errors (flux, pointing), missing CO flux due to the finite dish aperture, and the uncertainty of $\alpha_{\rm CO}$. Bolatto et al. (2013) summarized an uncertainty of ±0.3 dex (a factor of 2) for $\alpha_{\rm CO}$ in the disks of normal, solar metallicity star-forming galaxies. Therefore the total error on log $M_{\rm H_2}$ is about 0.4 dex. We do not adopt aperture correction for this SMT sample, since the angular sizes of the galaxies were carefully selected so that the SMT beam could effectively cover the CO emission region (their half-light radii are listed in Table 1), as CO emitting size is generally proportional to the optical size of disk galaxies (Lisenfeld et al. 2011).

We calculat the stellar masses with the SED fitting code `kcorrect` (version 4.2, Blanton & Roweis 2007). Provided a set of photometric data (in our case *ugriz* magnitudes), this code return stellar masses fitted from galaxy templates that based on stellar population synthesis models (Bruzual & Charlot 2003) using the Chabrier (2003) stellar initial mass function. For consistency we used this method to recalculate M_* for those SMT galaxies and the AMIGA-CO sample that have available SDSS DR9 data, and the results of the SMT sample is consistent with that provided by the JHU-MPA catalog. The COLD GASS survey has provided M_* data. $M_{\rm H_2}$, M_* of the SMT sample are listed in Table 2. The stellar mass for the 186 AMIGA-CO galaxies will be available online at *VizieR*.

4. RESULTS AND DISCUSSION

4.1. *Sample Comparison*

Among all kinds of galactic parameters, stellar mass (M_*) is the most fundamental and important one. The history of galaxy evolution is accompanied by the formation of stars from molecular gas and the cumulation of stars. So M_* is the first parameter being discussed along with H I and H_2 in the following sections. We use NUV$-r$ as an indicator of star formation activity, as it is well correlated with specific star formation rate (sSFR). The third parameter used in our analysis is *WISE* color W3$-$W2, which is similar to NUV$-r$ but less affected by dust attenuation.

First of all, we compare our SMT sample with the AMIGA and COLD GASS samples to explore their difference in physical properties. Figure. 1 shows the distributions of their stellar masses (M_*), concentration indices (R_{90}/R_{50}) and NUV$-r$. Comparing all galaxies from the three samples and including those undetected in CO, we find a few differences between the samples. First, the SMT sample is very similar to the AMIGA especially in M_* and R_{90}/R_{50} distributions, although its NUV$-r$ colors are slightly bluer than that of AMIGA on average, and AMIGA included a small portion of galaxies with red NUV$-r$ colors. Second, The COLD GASS galaxies show distinct properties than the SMT and AMIGA samples, that they are not only more massive ($M_* \geq 10^{10} M_\odot$), but also tend to be more bulge-dominated (higher R_{90}/R_{50} values) and redder in NUV$-r$. However, if we only compare those galaxies with secure CO detections (thicker histograms in Figure. 1), the differences between the three samples become less prominent, since most of the undetected galaxies are red and budge-dominated. The NUV$-r$ distribution shows that the COLD GASS contained some red galaxies, which are probably in accordance with those in the middle panel that have high R_{90}/R_{50} values. These undetected galaxies should be early-type massive galaxies that have a predominant stellar bulge, and quiescent in star formation since they contain little molecular gas.

Figure. 2 shows the normalized distributions of $M_{\rm H_2}$ and $M_{\rm H\,I}$ of the three samples. It is interesting to see that although they share a common distribution in $M_{\rm H\,I}$, their $M_{\rm H_2}$ distributions are different. The highest $M_{\rm H_2}$ in each sample are similarly at $\sim 10^{10.2} M_\odot$, but the COLD GASS galaxies have higher mean $M_{\rm H_2}$ and narrower $M_{\rm H_2}$ distribution. Looking into the samples and we found that, among all the galaxies studied in this paper, only seven galaxies with $M_{\rm H_2} \leq 10^{8.5} M_\odot$ are massive galaxies ($M_* \geq 10^{10} M_\odot$). So the reason we do not see low $M_{\rm H_2}$ ($\leq 10^{8.4} M_\odot$) in the COLD GASS sample is because M_* is proportional to $M_{\rm H_2}$, and those galaxies with low $M_{\rm H_2}$ are most likely low M_* galaxies that were missed by the COLD GASS sample, and such galaxies can only be studied when samples are extended down to low M_* regime. On the other hand, the lower panel of Figure. 2 shows that, although the three samples have different M_* distributions, they appear to show similar $M_{\rm H\,I}$ distributions. As a consequence, our SMT sample and the AMIGA-CO sample span a wider $M_{\rm H_2}$ range than the COLD GASS did, and such difference will play a role in our analysis of the $M_{\rm H_2}/M_{\rm H\,I}$ ratios (Section 4.3).

4.1.1. *WISE color diagram*

The *WISE* all-sky near-to-middle infrared catalog with high sensitivity provides large and homogenous samples for exploring the relationship between gas (H_2 and H I) and infrared emission of galaxies. Here we compare the infrared properties derived from the *WISE* catalog of the three samples.

In Figure. 3 we plot the color-color diagram (W1 $-$ W2 as a function of W2 $-$ W3) for the whole combined sample, including those sources with only tentative or non-detection of CO. With the annotation of different kinds of sources on the diagram (see Wright et al. 2010), it is obvious that those galaxies without significant CO detection are more likely ellipticals, and they tend to have 'bluer' W2 $-$ W3 colors (W2 $-$ W3 $\lesssim 2$). In contrast, for galaxies detected in CO, there is a good consistency in *WISE* colors of massive galaxies and intermediate-M_* galaxies, that they confined in a quite small area on the diagram. The CO detected galaxies tend to be 'redder' in W2 $-$ W3 color, and such difference resembles that in the NUV$-r$ color (Figure. 1). The W2 $-$ W3 color has been suggested to be a useful star-forming indicator (Donoso et al. 2012), in the context that W4 band is much less sensitive comparing with the other bands so

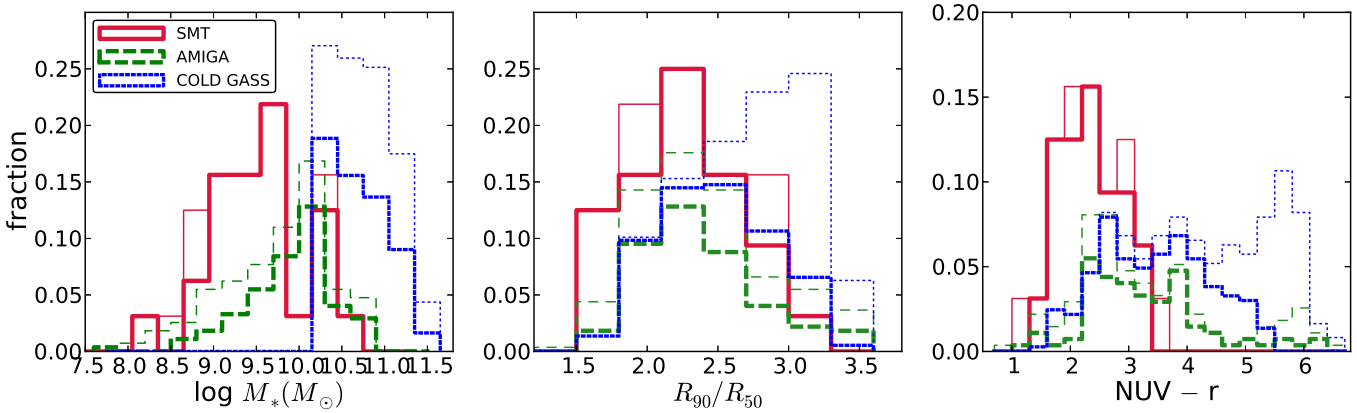

Figure 1. Normalized distributions of stellar mass M_*, concentration indices R_{90}/R_{50} and NUV−r color of the three samples used in this paper. Blue dotted histograms represent the COLD GASS survey of massive galaxies ($M_* \geq 10^{10} M_\odot$). Red solid and green dashed histograms represents the SMT sample and the AMIGA-CO, respectively. The histograms of thin lines denote the entire sample, while thicker histograms denote only those galaxies with secure CO detections (S/N $\geq$ 5). For clarity, in the first panel the SMT and COLD GASS are slightly offset with respect to the AMIGA.

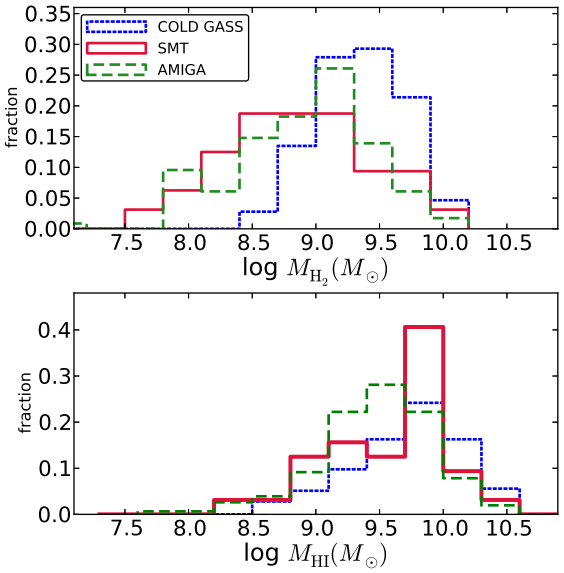

Figure 2. Normalized distributions of molecular gas masses ($M_{\rm H_2}$) and atomic gas masses ($M_{\rm H\,I}$) of the three samples used in this paper. Blue histograms represent the COLD GASS survey of massive galaxies ($M_* \geq 10^{10} M_\odot$). Red solid and green dashed histograms represent our SMT sample and the AMIGA sample, respectively. The COLD GASS has narrower $M_{\rm H_2}$ distribution, and the three samples are similar in the $M_{\rm H\,I}$ distribution.

W4 data would not be available for as many galaxies as the other three bands are. In fact, we found that the detection rate of CO has good correspondence with the W3 S/N, i.e., for both the COLD GASS and AMIGA-CO, among those galaxies with CO S/N $\geqslant$ 5, only two sources have W3 S/N $<$ 10.

In the COLD GASS sample, three galaxies can be classified as AGN, based on the *WISE* color criteria, W1 − W2 $>$ 0.8, which has been demonstrated to be capable of selecting strong AGN/QSOs (Yan et al. 2013). Moreover, eight COLD GASS galaxies were classified as ULIRGs (two of them are also AGN based on the W1 − W2 criteria), and this diagram shows that these AGN/ULIRGs have nearly the reddest IR colors among the whole combined sample, since their IR spectrum energy distribution (SED) peaks towards longer wavelength due to the contribution of hot dust emission originated from AGN or intense starburst. Because the IR emission in AGN host galaxies is severely contaminated, and deviates from normal galaxies whose IR emission is mainly contributed by stellar populations, we exclude these AGNs in the discussion of the relation between molecular gas and IR luminosities.

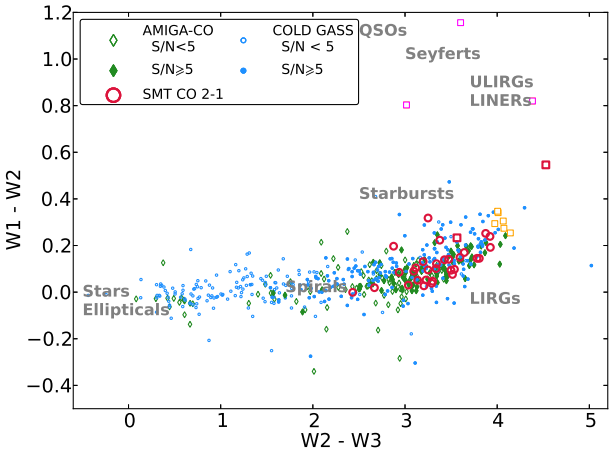

Figure 3. W1−W2 (3.4 μm −4.6 μm) vs. W2−W3 (4.6 μm − 12 μm) color-color diagram. Red big circles and squares represent the SMT sample (squares are (U)LIRGs), green diamonds and blue dots represent the AMIGA-CO and COLD GASS samples, respectively. Empty diamonds and dots show those galaxies without secure detections. Orange squares are COLD GASS (U)LIRGs, and magenta squares are AGNs classified based on the criteria W1−W2 $>$ 0.8. Text annotations inside are *WISE* sources classification (Wright et al. 2010).

4.2. *Gas fraction scaling-relations*

In Figure. 4 we plot the scaling-relations between gas fraction $M_{\rm gas}/M_*$ (in this paper it refers to $f_{\rm H_2} \equiv M_{\rm H_2}/M_*$ and $f_{\rm HI} \equiv M_{\rm H\,I}/M_*$) and several galactic properties, M_*, NUV−r and W3−W2 colors, for our SMT sample, the AMIGA-CO sample, and the COLD GASS sample. Comparing with AMIGA and COLD

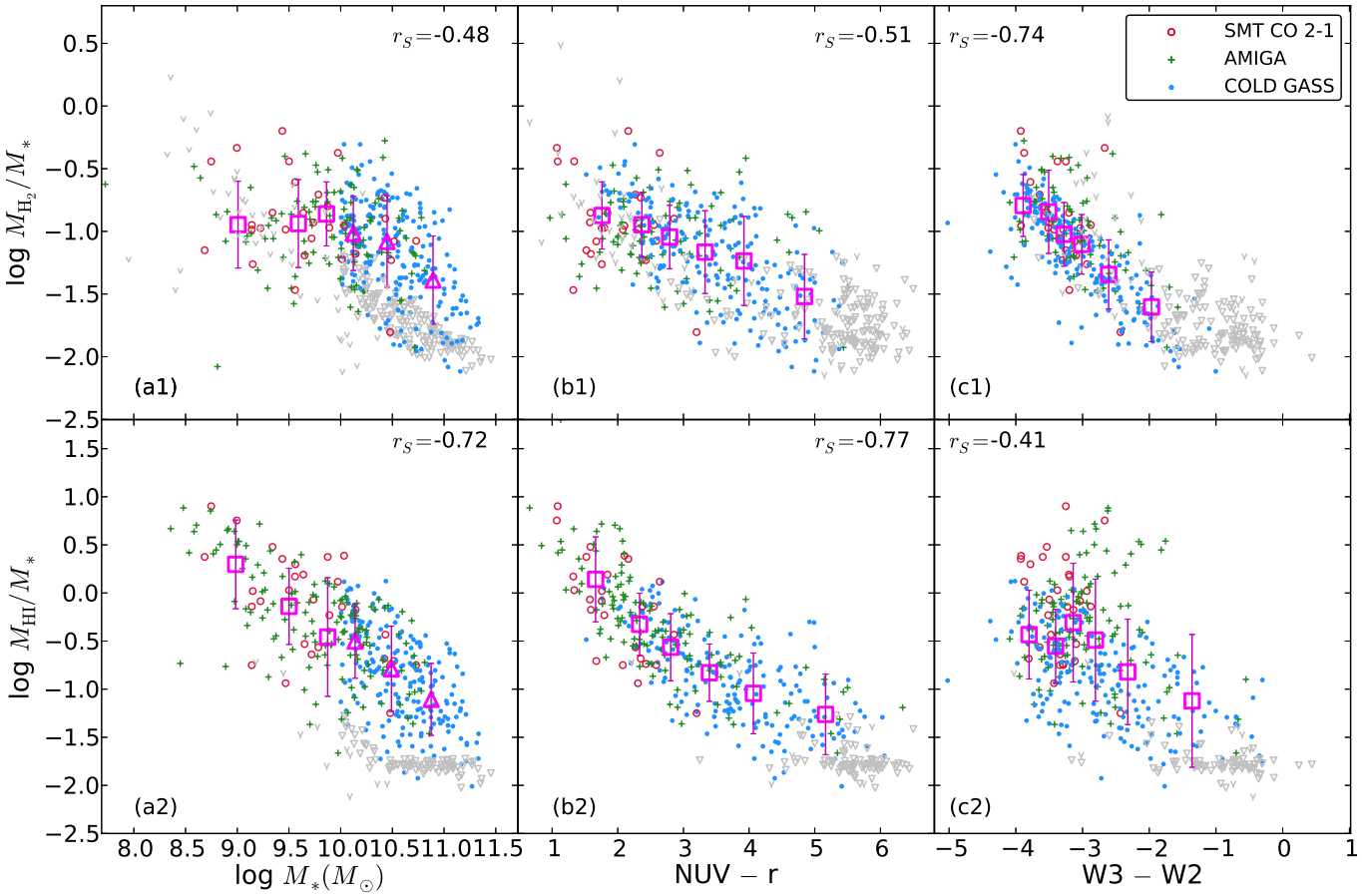

Figure 4. Scaling-relations of gas fraction ($M_{\rm H_2}/M_*$ and $M_{\rm H\,I}/M_*$) as a function of M_*, NUV−r and W3−W2 (12 μm −4.6 μm), respectively. Red circles, green crosses and blue dots represents our SMT sample, AMIGA-CO and COLD GASS, respectively. Dark gray triangles and light gray open arrows show gas fraction upper limits of COLD GASS and AMIGA, respectively. Gray solid lines are the linear fitting of the SMT and AMIGA-CO combined sample, with the Spearman correlation coefficient $r_{\rm S1}$ shown in each panels. Blue dashed lines are the linear fitting for the COLD GASS sample, with the Spearman correlation coefficient $r_{\rm S2}$ shown in each panel. Only secure detections (S/N $\geq$ 5) are included in the fitting. In panel (a1) and (a2) the averaged log $M_{\rm H_2}/M_*$ and log $M_{\rm H\,I}/M_*$ along with their scatters are showed with magenta squares, each bin having same number of galaxies. While log $M_{\rm H\,I}/M_*$ is obviously higher in lower mass galaxies, the trend of increasing log $M_{\rm H_2}/M_*$ with decreased M_* is very weak.

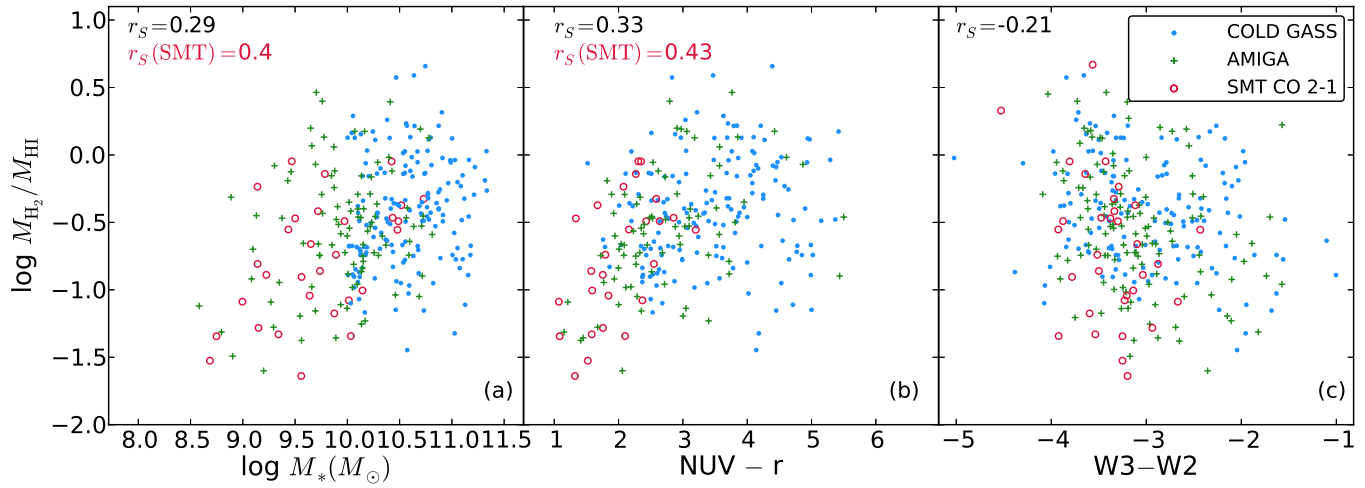

Figure 5. Scaling-relations of gas ratio ($M_{\rm H_2}/M_{\rm H\,I}$) as a function of M_*, and NUV−r and W3−W2, respectively. Red circles, green crosses and blue dots represent our SMT sample, AMIGA-CO and COLD GASS, respectively. The Spearman correlation coefficient $r_{\rm S1}$ in each panel are for the SMT and AMIGA-CO combined sample, and $r_{\rm S2}$ are for the COLD GASS massive sample.

GASS, our SMT observations have provided a well selected sample which extends to lower stellar mass regime. To explore the relationship between *WISE* infrared color and gas fractions, and to compare the infrared color with NUV−r, we use the color W3−W2 so that it is consistent with the optical color NUV−r, in the sense that galaxies with greater W3 − W2 values correspond to"red", indicating the emission is dominated by old stellar population, while "blue" indicating the emission is dominated by young stars arising from on-going star formation. Note the difference from the traditional form W2−W3 used in Figure. 3 and literatures (e.g., Donoso et al. 2012). The Spearman correlation coefficients are showed on each panels.

In Figure. 4(a1) we plot $f_{\rm H_2}$ as a function of M_*, and in Figure. 4(a2) $f_{\rm HI}$ as a function of M_* (in log-log scale). Combining the different samples allows the relation between $f_{\rm gas}$ and M_* can be explored in the range between $M_* \sim 10^8 M_\odot$ and $\sim 10^{11.5} M_\odot$. These two panels show two major differences between $f_{\rm H_2}$ and $f_{\rm HI}$: First, $f_{\rm HI}$ obviously increases with decreasing M_*, and in the low M_* end $f_{\rm HI}$ can reach as high as almost 10, while $f_{\rm H_2}$ is always lower than unity. In the massive galaxies $f_{\rm H_2}$ significantly decreases with increasing M_*, but in low to intermediate M_* galaxies the mean $f_{\rm H_2}$ seem unchanged (see following paragraph). Such difference indicates that in low mass systems, most of their gas mass are in the form of H I, while their $M_{\rm H_2}$ are always less than M_*. Second, log $f_{\rm HI}$ anti-correlates much better with log M_* than log $f_{\rm H_2}$ does. In the stellar mass range between about 10^8 $M_\odot$ to 10^{11} $M_\odot$, $f_{\rm HI}$ decreases with increasing M_* with a universal slope and the correlation is quite prominent ($r_s = -0.72$ for the entire sample), while in Figure. 4(a1) the scatter is larger, and the Spearman coefficient is lower ($r_s = -0.48$). It is intriguing to notice that the scatter of the COLD GASS sample in panel (a1) and (a2) are quite similar, and the two figures are mainly different in the low to intermediate M_* galaxies, which may imply that the properties of cold gas content change quickly in galaxies of intermediate M_*, likely accompanying the transitions from H I to H_2.

To check the mean relations for the intermediate-M_* sample in Fig 4(a1) and (a2), we also plot the bin averaged log $f_{\rm H_2}$ and log $f_{\rm HI}$ (magenta squares), with nearly the same amount of sources in each M_* bin. It is interesting that the averaged $f_{\rm H_2}$ in low mass galaxies ($M_* < 10^{10} M_\odot$) seem unchanged, while the decreasing trend of the averaged $f_{\rm HI}$ with increasing M_* is more prominent, with much smaller scatter. The results of COLD GASS survey showed that the trend of decreased $f_{\rm H_2}$ with increasing M_* becomes steeper at M_* $> 10^{10.5} M_\odot$ (Tacconi et al. 2013, and references therein), and in our work the mean $f_{\rm H_2}$ at $M_* \sim 10^{10} M_\odot$ is similar to that given by the COLD GASS (7%). The trend of increasing $f_{\rm H_2}$ with decreasing M_* is able to be extended down to $M_* \sim 10^8 M_\odot$, thus we confirm that the trend becomes much shallower in lower mass galaxies. It is interesting that our result is not only consistent with that of the COLD GASS, but also agrees with the scenario predicted by semi-analytical models (Fu et al. 2012), that the $f_{\rm H_2}$ in low mass galaxies ($M_* < 10^{10.2} M_\odot$) differ not too much.

Since most of the galaxies in these plots are normal galaxies, it is natural to see a similarity in their moderate $f_{\rm H_2}$, because high $f_{\rm H_2}$ is likely to occur in LIRGs and/or starburst systems. Panel (a2) shows that our SMT sample selected from the ALFALFA catalog seems to follow the same relation between $f_{\rm HI}$ and M_* as the other galaxies, although Huang et al. (2012) have demonstrated that the ALFALFA population are generally more gas-rich than other samples such as the GASS. The very high $f_{\rm HI}$ in low M_* galaxies indicates that these systems had little integrated past star formation, and they have been very inefficient in converting their gas into stars (Huang et al. 2012; Blanton & Moustakas 2009). Because their H I is more abundant than H_2 (see Figure. 5 and following discussions), we speculate that they were mainly inefficient in the process of converting H I to H_2 and forming molecular clouds.

In Figure. 4(b1) and (b2) we explore how $f_{\rm H_2}$ and $f_{\rm HI}$ relate with NUV−r color, respectively. Since UV emission originates from young stars and r-band emission is mainly contributed by old stars, NUV−r is strongly correlated with specific-SFR (sSFR, Huang et al. 2012), hence a good tracer of star-forming activities. It is natural to see in panels (b1) and (b2) that $f_{\rm H_2}$ and $f_{\rm HI}$ both depend on NUV−r, that $f_{\rm gas}$ is obviously higher in blue galaxies. First of all, compared with Saintonge et al. (2011a), we have provided in panel (b1) more low M_* galaxies that are bluer in NUV−r. Although in low mass galaxies the dust-to-gas ratio is suggested to be less due to their lower gas-phase metallicities (Blanton & Moustakas 2009), we do not see any significant difference between the samples in the relation between log $f_{\rm H_2}$ and NUV−r. With respect to the red end, Saintonge et al. (2011a) have found that in COLD GASS galaxies the CO detection rates significantly dropped at NUV−r $\gtrsim 5$, which implied a $f_{\rm H_2}$ threshold and very little H_2 content in those red and quiescent systems. Second, we show in Figure. 4(b2) that in the bluest star forming galaxies, the decreasing trend of $f_{\rm HI}$ with NUV−r is steeper than that in the red galaxies, which are mostly massive. This is consistent with the result of Catinella et al. (2012) that H I-rich galaxies deviate from the mean relation defined by galaxies with "normal" H I content, and the reason for this deviation and the scatter might be the scenario that the UV emission in red galaxies is contributed by more evolved stellar populations, and their UV emission might not be well associated with H I. Another reason of the non-linearity was some of the galaxies with very low gas fractions were missed in the GASS survey (Catinella et al. 2012), and panel (b2) shows that our sample provides more galaxies with higher $f_{\rm HI}$, thus the non-linearity is more obvious. Third, it is interesting that log $f_{\rm HI}$ correlate with NUV−r better than log $f_{\rm H_2}$ does. It is probably because H_2 resides in the central region of galaxies, where UV emission is easily absorbed due to dense dust content, while on the other hand H I dominates the outskirt of galactic disks, where most of the UV emission can be observed (Saintonge et al. 2011a).

To address this issue, in Figure. 4(c1) and (c2) we plot $f_{\rm H_2}$ and $f_{\rm HI}$ as a function of *WISE* infrared color W3−W2, which is another color parameter but it is much less affected by dust attenuation than NUV−r or other optical colors. The W2 (4.6 μm) near-infrared band is a good tracer of stellar mass, and W3 (12 μm) mid-infrared band covers the 11.3 μm PAH and can also be contributed

by the dust continuum emission at 12 μm. NUV$-r$ has been widely used to indicate galactic star formation activities and classify galaxies into blue cloud or red sequence, and W2$-$W3 color has also been suggested to be a good star formation indicator (Donoso et al. 2012). Here we compare their relations with $f_{\rm H_2}$ and $f_{\rm HI}$. Panel (c1) shows a clear correlation between $f_{\rm H_2}$ and W3$-$W2, and the dependence of $f_{\rm H_2}$ on W3$-$W2 ($r_s = -0.74$) is much stronger than that on NUV$-r$. Panel (c1) also shows that, most of the sources without positive CO detection are red in W3$-$W2, and none of the galaxies with W3$-$W2 > -1 were detected. These "red" galaxies seem to lie above the relation defined by those "blue" galaxies, which might indicate that the $f_{\rm H_2}$ upper limits of the red galaxies were probably overestimated, which is consistent with that suggested by Saintonge et al. (2011a), where by stacking the undetected spectra they found a mean $f_{\rm H_2}$ less than 0.16%. Figure. 4(c1) allows us to confirm that the scatter between $f_{\rm H_2}$ and NUV$-r$ is mainly caused by dust attenuation, and by introducing the new infrared color W3$-$W2, we show that $f_{\rm H_2}$ has a better correlation with W3$-$W2. Since the sample used in this work are mostly star-forming galaxies, their 12 μm emission is contributed by both PAH and dust continuum which originates from current star forming activities, while their W2 (4.6 μm) emission is mainly contributed by stellar components. In addition, the mass of their star-forming gas (dense molecular gas) should be proportional to the overall gas content traced by CO, therefore we can see this strong correlation between $f_{\rm H_2}$ and W3$-$W2.

Then in Figure. 4(c2) we plot log $f_{\rm HI}$ as a function of W3$-$W2, and the result shows that, the COLD GASS sample appears to be distinct from the other two samples, and only in the COLD GASS sample log $f_{\rm HI}$ has a weak dependence on W3$-$W2, whereas the scatter in the other two samples is much larger. There are some galaxies which tend to be redder than the mean relation (magenta squares), and comparing with panel (a2) it is obvious that those offset sources are mainly low mass galaxies. This may indicates the large diversity of star formation efficiencies in these low M_* systems. On the one hand, as already mentioned above, there is a large amount of H I in some of the low M_* systems but they have been inefficient in converting their H I into H_2 and stars, and since infrared emission originates from dust which mixes with both atomic and molecular gas (Bohlin et al. 1978) , we do not see a good correlation between $f_{\rm HI}$ and W3$-$W2 in low M_* galaxies. On the other hand, in massive galaxies, they have more consistent star formation efficiencies and consume the gas constantly thus we see a correlation between $f_{\rm HI}$ and infrared color. Another possible explanation for the deviation of those high $f_{\rm HI}$ galaxies in panel (c2) is that in low M_* galaxies there might be little PAH emission due to their low metallicities, and comparing with massive galaxies more abundant in PAH, W3 emission of low mass systems would be contributed less by the 11.3 μm PAH, so they are prone to be redder.

In summary, the correlations between $f_{\rm gas}$ and the two colors, NUV$-r$ and W3$-$W2, are consistent with a galaxy evolution picture that low mass galaxies are more gas rich and especially abundant in H I, but they are inefficient in converting their H I into H_2 molecular clouds then stars; in massive galaxies the star forming efficiency is more consistent and there is less molecular gas since it has been consumed in forming stars, while the overall decreased gas amount causes a drop in the overall gas density, and reduce the rate of transforming H I into H_2, with certain amount of gas can remains in the form of H I, and some of the H I can be either replenished or accreted from the environment recently, if not expelled by the interaction between nearby galaxies.

4.3. *H_2-to-H I gas ratio*

In the previous section we discuss how gas fractions $f_{\rm H_2}$ and $f_{\rm HI}$ depend on galactic properties, respectively. It is also worth exploring the scaling relations between $M_{\rm H_2}/M_{\rm H\,I}$ and global physical parameters, because the relationship between H_2 and H I in galaxies is a fundamental question, yet how this relation is affected or regulated by other galactic properties is still unclear. As already discussed in Young & Scoville (1991) and recently in the AMIGA survey (Lisenfeld et al. 2011), the ratio of $M_{\rm H_2}/M_{\rm H\,I}$ declines in late type galaxies, because of more H I content in late type galaxies than early type (such as S0, Sa Hubble type). Saintonge et al. (2011a) also found that log $M_{\rm H_2}/M_{\rm H\,I}$ decreases with increasing R_{90}/R_{50}, but the $M_{\rm H_2}/M_{\rm H\,I}$ ratio has a quite large scatter in different galaxies, although $M_{\rm H_2}$ is proportional to $M_{\rm H\,I}$ as expected (Saintonge et al. 2011a).

In Figure. 5 we plot the scaling-relations between gas ratio (log $M_{\rm H_2}/M_{\rm H\,I}$) and the same parameters used in Figure. 4, M_*, NUV$-r$ and W3$-$W2. The plots show that the dependence of log $M_{\rm H_2}/M_{\rm H\,I}$ on these parameters are quite weak, and in the COLD GASS massive sample the scatter is large, which were already found in Saintonge et al. (2011a) and can be explained by the large scatter of log $f_{\rm H_2}$ and log $f_{\rm HI}$ in Figure. 4. However, it is interesting to see in panels (a) and (b) that for our SMT galaxies, log $M_{\rm H_2}/M_{\rm H\,I}$ appears to correlate with log M_* ($r_s = 0.4$) and NUV$-r$ ($r_s = 0.43$), although the color of the SMT sample tend to be blue (NUV$-r < 4$). The $M_{\rm H_2}/M_{\rm H\,I}$ ratio tend to be higher in more massive and/or relatively redder galaxies of the SMT sample. We do not find any significant correlation between log $M_{\rm H_2}/M_{\rm H\,I}$ and W3$-$W2, which should be resulted from the large scatter and the non-linear relation between $f_{\rm HI}$ and W3$-$W2. The $M_{\rm H_2}/M_{\rm H\,I}$ in the SMT sample are in the range of about 0.02 – 4.7, and only in the two LIRGs their $M_{\rm H_2}/M_{\rm H\,I}$ are greater than unity, indicating more H_2 than H I, but in all the other normal galaxies the $M_{\rm H\,I}$ are heavier than $M_{\rm H_2}$. The trend in Figure. 5a confirmed what was suggested in the SINGS survey that $M_{\rm H_2}/M_{\rm H\,I}$ declined at lower M_* (Blanton & Moustakas 2009). And $M_{\rm H_2}/M_{\rm H\,I}$ seems to increase in moderate NUV$-r$ color, is due to the decreasing $f_{\rm HI}$ in red galaxies that is shown in Figure. 4(a2).

Consider Figure. 5 with Figure. 4 together, we speculate that, $M_{\rm H_2}/M_{\rm H\,I}$ increases as increasing M_* in lower M_* galaxies, is an implication of the dependence of H I-to-H_2 transition on the M_* cumulation in galaxies. In the history of galaxy evolution, consuming gas to form stars is accompanied by the accretion of surrounding diffuse gas which is mainly in atomic form (H I), and star-formation is also accompanied by the transformation from H I into H_2 (Krumholz 2013). On the early (young) stage, there was enough H I to be converted into H_2 then molecular clouds, wherein star formed and the $M_{\rm H_2}/M_*$

fraction remained at a certain level (intermediate–M_* in Figure. 4(a1)); on a later stage, when a galaxy became more massive (in M_*) its sSFR (NUV−r) increase, then its H I probably become deficient (Figure. 4(a2)) as most of the H I were transformed into molecular clouds, and then the stellar mass kept growing but molecular gas fraction would decrease (massive galaxies in Figure. 4(a1)). Despite the large scatter in our plots, this scenario of the evolution of H I, H_2 and M_*, is a possible explanation of the plausible turnover of f_{H_2} at M_* $\sim 10^{10} M_\odot$. We should note two major sources of the large scatters in these relations, one is the different star forming history and environment of different galaxies, and the other is the larger uncertainty of α_{CO}, especially in different kinds of galaxies, which brings in large scatter in the conversion from CO flux to M_{H_2}. while COLD GASS used a different α_{CO} for the 12 ULIRGs ($1.0\ M_\odot(\mathrm{K\,km\,s^{-1}\,pc^2})^{-1}$), the M_{H_2} of all other galaxies in the combined sample were calculated based on a universal α_{CO}. We do not discuss the details of the calibration of α_{CO} in different kinds of galaxies, such as nearby normal galaxies, dwarfs, or LIRGs, as other studies have been focusing on this topic (e.g., see Bolatto et al. 2013; Sandstrom et al. 2013). Therefore the large scatter we see in these scaling-relations is largely intrinsic thus might not be reduced easily at this stage.

4.4. *The relationship between M_{H_2} and 12 μm*

The tight anti-correlation shown in Figure 4(c1) implies that M_{H_2} might be well correlated with 12 μm emission, since M_* can be traced by the 4.6 μm (W2). In this section we discuss the relation between molecular gas mass M_{H_2}, and the *WISE* 12 μm emission. Donoso et al. (2012) has found that 12 μm is a good tracer of star formation especially in young galaxies, so relate 12 μm with M_{H_2} is essentially the same question as the traditional Kennicutt-Schumit law (K-S law), which related the SFR surface density (Σ_{SFR}) and gas surface density (Σ_{gas}) and has been one of the most important topics in astrophysics (Kennicutt 1998; Schmidt 1963; Kennicutt & Evans 2012). We will not go into details of this complicate topic in this paper, instead we only discuss how $L_{12\,\mu m}$ relates with M_{H_2}, and to what extend can we use $L_{12\,\mu m}$ to trace M_{H_2}, at least for a certain type of galaxies. Although the W4 band (22 μm) of *WISE* suffers from relatively poor sensitivity and sparse resolution, the W3 band data still have a potential for the study of SF in galaxies.

In Figure. 6 molecular masses M_{H_2} are plotted as a function of W3 (12 μm) luminosities $L_{12\,\mu m}$. Including in panel (a) only those galaxies with high S/N in both CO 1-0 detection and W3 magnitude (S/N $\geqslant$ 5), we find that log M_{H_2} is strongly correlated with log $L_{12\,\mu m}$ in all the samples. There are A few AGNs and (U)LIRGs of the COLD GASS sample (red and orange squares in panel a) significantly deviate from the mean relation, which is probably because their near-to-mid infrared emission is enhanced by the warmer dust temperature due to AGNs and/or intense starburst. We excluded these AGNs and (U)LIRGs in the fitting, and panel (a) shows that the COLD GASS sample has a smaller scatter comparing with the AMIGA-CO. This might be a result from the difference in the angular sizes of galaxies of the two samples. Since the COLD GASS limited the galaxy distance to be larger than 100 Mpc, galaxies that are too large for the observations are effectively excluded, and aperture effect did not induce significant scatter in this plot, although some of the galaxies might be still larger than both the IRAM 30-m beam and the *WISE* aperture. On the other hand, the AMIGA sample suffers from the aperture effect because of the smaller distances of galaxies and different instruments used in the CO observations. First, the AMIGA included very nearby galaxies as close as a few Mpc, and since the *WISE* W3 band photometry was performed with finite apertures (the maximal aperture adopted is $\sim 25''$), the data for those very nearby galaxies only covered a small portion

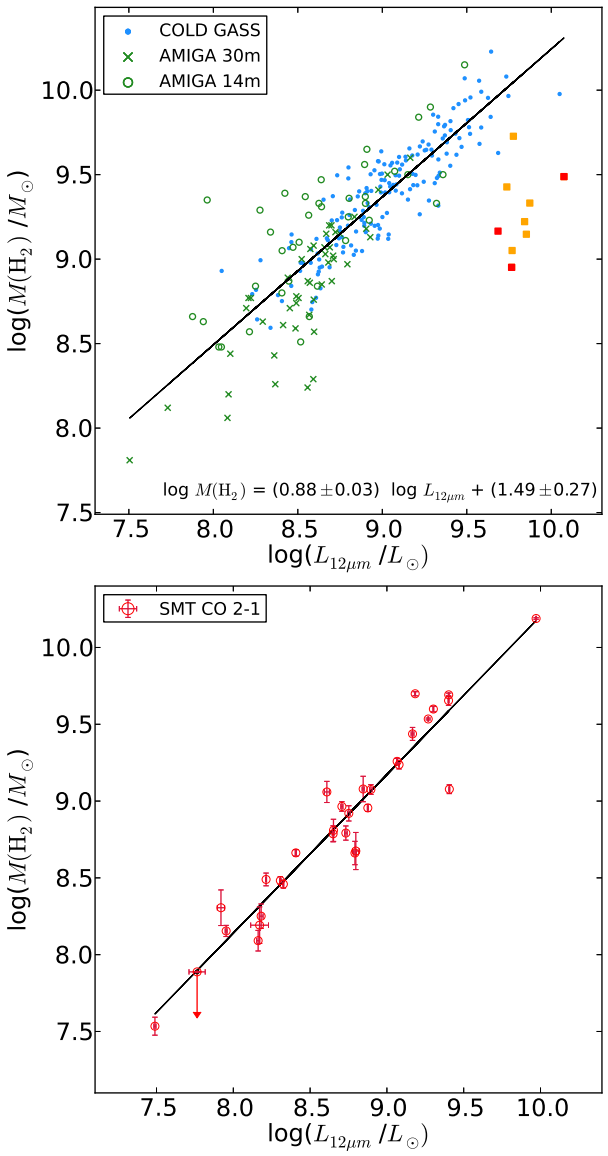

Figure 6. Upper panel shows the relation between log M_{H_2} and $L_{12\,\mu m}$ for the CO 1-0 measurement from the AMIGA sample and COLD GASS sample. Blue dots denote the COLD GASS, green crosses denote the AMIGA sample which were observed with 30-m telescope, and green circles denote those observed with 14-m telescope. Orange squares are COLD GASS (U)LIRGs and red squares are AGNs, and they are excluded from the fitting, which is shown as the black solid line. Lower panel shows the same plot for the SMT CO 2-1 sample.

of the galaxy hence larger uncertainties in both their CO and 12 μm fluxes which were very likely underestimated. Second, the AMIGA compiled the CO sample with data from different telescopes with different HPBW (21″ for the IRAM 30-m, and 45″ for the FCRAO 14-m, respectively), and the W3 photometry aperture is much smaller than the HPBW of the 14-m telescope so the W3 data were actually collected from smaller spatial regions than that of the CO data thus W3 emission was very likely underestimated.

In panel (a) we plot the AMIGA galaxies with different symbols according to the telescopes they were observed with, IRAM 30-m (green crosses) or FCRAO 14-m (green circles). And the plot shows that the aperture effect causes most of the AMIGA galaxies that were observed with the 14-m telescope to be weaker in $L_{12\,\mu\mathrm{m}}$, because the relatively small W3 aperture underestimated their $L_{12\,\mu\mathrm{m}}$, and some AMIGA galaxies which were observed with the 30-m galaxies tend to have smaller $M_{\mathrm{H_2}}$ because the small beam of the 30-m telescope underestimated their CO fluxes. These two aspects of the AMIGA-CO sample together brought large scatter in panel (a), but the overall correlation between log $M_{\mathrm{H_2}}$ (derived from CO 1-0) and log $L_{12\,\mu\mathrm{m}}$ is still quite strong (Spearman coefficient $r_s = 0.90$). A least square linear fit for Figure. 6a yields:

$$\log M_{\mathrm{H_2}}(\mathrm{CO}_{1-0}) = (0.88\pm0.03)\log L_{12\mu\mathrm{m}} + (1.49\pm0.27) \quad (3)$$

with a correlation coefficient $r = 0.88$.

Figure. 6b shows the same plot for the SMT sample, whose $M_{\mathrm{H_2}}$ were converted from the CO 2-1 data. The correlation turnes out to be even stronger than that in panel (a). Although the sample size is smaller than the CO 1-0 sample shown in panel (a), our sample selection has excluded those galaxies that are interacting systems or too extended for the observation, and the result shows that such criterion effectively alleviate the aperture effect (see the Appendix for more discussion). A least square linear fit for Figure. 6b yields:

$$\log M_{\mathrm{H_2}}(\mathrm{CO}_{2-1}) = (1.03\pm0.06)\log L_{12\mu\mathrm{m}} + (-0.12\pm0.48) \quad (4)$$

with a correlation coefficient $r = 0.96$ ($r_s = 0.94$). It is intriguing that the slope is very close to unity, suggesting that the $M_{\mathrm{H_2}}$ traced by CO 2-1 is nearly proportional to $L_{12\,\mu\mathrm{m}}$. This slope is slightly larger than that derived from CO 1-0 in panel (a), which can be contributed by two effects. The first effect might be the influence of the aperture effect, as mentioned above some galaxies in the CO 1-0 sample in panel (a) were too extended and the measurements of their $M_{\mathrm{H_2}}$ and/or $L_{12\,\mu\mathrm{m}}$ has large uncertainties, which might affect the fitted slope, while the SMT CO 2-1 sample suffer much less from the aperture effect since they were carefully selected. The second effect is probably the difference between the two CO transitions. Observations in nearby galaxies have provided a mean CO 2-1 to CO 1-0 line ratio R21 = 0.7 (Leroy et al. 2013), and CO 2-1 has been demonstrated to be a reliable $M_{\mathrm{H_2}}$ tracer. However, the excitation condition in different galaxies would induce scatter in R21, especially in galaxies with different star forming activities. In more active star-forming galaxies, the H_2 is more abundant and the gas temperature is higher so CO line would tend to be saturated hence a higher R21, while in quiescent galaxies if the temperature is very low ($\sim$ 5K) the CO 2-1 would be less excited and R21 is lower, thus their $M_{\mathrm{H_2}}$ is possibly underestimated with CO 2-1. Therefor this effect can cause the slope in Figure. 6b to be higher, and we consider this the major influence.

This correlation resembles the K-S law, in which SFR can be calculated using total infrared luminosity L_{IR}, which is usually integrated from 12 μm to 100 μm IRAS data. So the correlation between $M_{\mathrm{H_2}}$ and $L_{12\,\mu\mathrm{m}}$ is anticipated, since in star-forming galaxies their infrared spectral energy is dominated by young stellar populations (Donoso et al. 2012). Moreover, the W3 band is very sensitive to polycyclic aromatic hydrocarbon (PAH) emission at 11.3 μm and amorphous silicate absorption (10 μm) in nearby star-forming galaxies (Wright et al. 2010). The 11.3 μm PAH emission was found to be spatially well correlated with CO emission in high resolution observation towards nearby star-forming galaxies (Wilson et al. 2000), and Figure. 6 shows a consistent relation on the global scale. Clemens et al. (2013) also suggested that the dust mass in a galaxy is proportional to its ISM content in general. One might expect that the *WISE* W4 band would improve this relation as 24 μm should trace star formation better than other near- or mid-infrared bands, but substituting W4 for W3 in Figure. 6b does not improve the correlation, and shows larger scatter. We believe this is due to the fact that comparing to the other three bands, *WISE* W4 band suffers from much poorer sensitivity, more sparse resolution and sometimes saturated images, thus for the study of extragalactic subjects that require sensitive and accurate photometric measurements, W4 is not as useful as the other three bands.

The significance of this correlation between 12 μm emission and $M_{\mathrm{H_2}}$ is that it indicates the potential application of W3 data in the prediction of molecular gas content of galaxies, which would be useful considering that *WISE* provides all-sky catalog for galaxies and it is much more sensitive than the IRAS, whose infrared catalog has been widely used in observations to predict CO flux. Although the ALFALFA catalog will have H I data for up to $\sim$30,000 galaxies, large CO surveys to-day such as the COLD GASS have only measured hundreds of galaxies because of current technical restrictions, and CO surveys towards galaxies are still needed for investigating the molecular gas scaling relations. *WISE* W3 data can provide CO flux estimation for observations, and can even provide $M_{\mathrm{H_2}}$ prediction for the sake of statistics. Our results demonstrate that such prediction should be reliable at least for nearby star-forming galaxies selected from the ALFALFA- *WISE* matched sample. It should be noted that the sample used in our discussion are mainly star-forming galaxies, and careful treatment is still needed to verify whether this method of using $L_{12\,\mu\mathrm{m}}$ to trace $M_{\mathrm{H_2}}$ can be applied to other kinds of galaxies, such as early type galaxies, as 12 μm PAH emission can also originate from old stellar population, and in those galaxies without significant star forming activities, the 12 μm emission will be likely dominated by such old stars. We also caution that PAH is not an unambiguous tracer of star formation and such correlation might actually reflect that these galaxies share similar properties at 12 μm , which is contributed by both dust continuum and PAH emission. It would be interesting to study the behaviors of W3 emission in a variety of galaxy samples.

Further verification of this technique and its usage in the study of gas scaling relations in such large sample, will be addressed in future work.

5. SUMMARY

We selected a sample of 32 gas-rich normal star-forming galaxies from the ALFALFA-*WISE* matched sample, which span a stellar mass range between $\sim 10^{8-10.6} M_\odot$, and carried out CO 2-1 observations with the SMT 10-m telescope. We got high CO 2-1 detection rate and only one galaxy without significant CO detection (see Figure. 7). The calculated $M_{\rm H_2}$ and M_* are presented in Table 2.

CO 1-0 data are compiled from other galaxies surveys, the COLD GASS and AMIGA, and we use them along with our SMT sample to explore the gas scaling relations with $f_{\rm HI}$ and $f_{\rm H_2}$. The AMIGA-CO sample has similar properties as our SMT sample, in the sense that they share common M_*, R_{90}/R_{50} and NUV$-r$ distributions (Figure. 1), so combining the SMT sample with the AMIGA-CO sample allows us to improve the sample size of low- to intermediate-M_* galaxies($M_* < 10^{10}\ M_\odot$), and can be compared with the COLD GASS massive sample ($M_* > 10^{10}\ M_\odot$). Since we include a number of galaxies of low M_*, the dynamical range in plotting the relation between $f_{\rm H_2}$ and M_* as well as other galactic properties is enhanced comparing to the COLD GASS. Our main results include:

1. Bin-averaged $f_{\rm H_2}$ and $f_{\rm H_2}$ are derived for the whole sample, which shows that $f_{\rm HI}$ obviously increase in galaxies of lower M_*, while $f_{\rm H_2}$ almost keep unchanged in low- to intermediate-M_* galaxies ($M_* < 10^{10}\ M_\odot$). This result is consistent with that of the COLD GASS at similar M_* ($\sim 10^{10}\ M_\odot$), but we are able to extended it to lower M_* regime. We also induce a new parameter W3$-$W2 and compare the scaling relations between $f_{\rm gas}$ and two colors, NUV$-r$ and W3$-$W2, which are all star-forming indicators (Figure. 4). Our results show that while NUV$-r$ is anti-correlated with log $f_{\rm HI}$ tighter than $f_{\rm H_2}$, W3$-$W2 has tighter anti-correlation with log $f_{\rm H_2}$ than log $f_{\rm HI}$.

2. The gas ratio (log $M_{\rm H_2}/M_{\rm H\,I}$) scaling relations are also explored, and they all show large scatter (Figure. 5). This can be attributed to the scatter in the $f_{\rm H_2}$ and/or $f_{\rm HI}$ scaling relations. Only in the SMT sample we see correlations between log $M_{\rm H_2}/M_{\rm H\,I}$ and log M_* as well as NUV$-r$, that more massive and/or redder galaxies have higher $M_{\rm H_2}/M_{\rm H\,I}$.

3. We compare the relation between $M_{\rm H_2}$ and infrared properties derived from the *WISE* catalog, and find an excellent correlation between log $M_{\rm H_2}$ and log $L_{12\,\mu{\rm m}}$, the 12 μm luminosity. The slope of linear fittings of our SMT CO 2-1 sample is very close to unity (1.03$\pm$0.06), while the slope in the CO 1-0 sample is slightly shallower (slope = 0.88$\pm$0.03). Considering the *WISE* has provided all-sky data with high sensitive and has significant overlap with the ALFALFA H I catalog, one can use this relation to predict CO flux for observations, or even estimate $M_{\rm H_2}$ for a large amount of galaxies, at least for the ALFALFA-*WISE* matched sample which are dominated by gas-rich star-forming galaxies. Note that this method might not be used in galaxies dominated by old stellar populations, since a significant part of the 12 μm emission would originated from old stars thus no longer only trace young stars which are tightly correlated with molecular gas.

We thank the anonymous referee for careful review and valuable suggestions, the SMT staffs for their help during the observations, Ran Wang for her help with the observation, and U. Lisenfeld for kindly making the H I data available to us. X.J. acknowledges support for this work from the Strategic Priority Research Program "The Emergence of Cosmological Structures' of the Chinese Academy of Sciences (CAS), grant XDB09000000. This work is supported under the National Natural Science Foundation of China (grants 11273015 and 11133001), the National Basic Research Program (973 program No. 2013CB834905), and Specialized Research Fund for the Doctoral Program of Higher Education (20100091110009). Z-Y.Z acknowledges support from the European Research Council (ERC) in the form of Advanced Grant, COSMICISM. This publication makes use of data products from the Wide-field Infrared Survey Explorer, which is a joint project of the University of California, Los Angeles, and the Jet Propulsion Laboratory/California Institute of Technology, funded by the National Aeronautics and Space Administration. The Arecibo Observatory is part of the National Astronomy and Ionosphere Center which is operated by Cornell University under a cooperative agreement with the National Science Foundation. Based on observations made with the NASA Galaxy Evolution Explorer. GALEX is operated for NASA by the California Institute of Technology under NASA contract NAS5-98034. Funding for SDSS-III has been provided by the Alfred P. Sloan Foundation, the Participating Institutions, the National Science Foundation, and the U.S. Department of Energy Office of Science. The SDSS-III web site is `http://www.sdss3.org/`. SDSS-III is managed by the Astrophysical Research Consortium for the Participating Institutions of the SDSS-III Collaboration including the University of Arizona, the Brazilian Participation Group, Brookhaven National Laboratory, University of Cambridge, Carnegie Mellon University, University of Florida, the French Participation Group, the German Participation Group, Harvard University, the Instituto de Astrofisica de Canarias, the Michigan State/Notre Dame/JINA Participation Group, Johns Hopkins University, Lawrence Berkeley National Laboratory, Max Planck Institute for Astrophysics, Max Planck Institute for Extraterrestrial Physics, New Mexico State University, New York University, Ohio State University, Pennsylvania State University, University of Portsmouth, Princeton University, the Spanish Participation Group, University of Tokyo, University of Utah, Vanderbilt University, University of Virginia, University of Washington, and Yale University.

REFERENCES

Bigiel, F., Leroy, A. K., Walter, F., et al. 2011, ApJ, 730, L13

Blanton, M. R., & Moustakas, J. 2009, ARA&A, 47, 159
Blanton, M. R., & Roweis, S. 2007, AJ, 133, 734
Bohlin, R. C., Savage, B. D., & Drake, J. F. 1978, ApJ, 224, 132
Bolatto, A. D., Wolfire, M., & Leroy, A. K. 2013, ARA&A, 51, 207
Bouwens, R. J., Illingworth, G. D., Labbe, I., et al. 2011, Nature, 469, 504
Bruzual, G., & Charlot, S. 2003, MNRAS, 344, 1000
Calzetti, D., Kennicutt, R. C., Engelbracht, C. W., et al. 2007, ApJ, 666, 870
Carilli, C. L., & Walter, F. 2013, ARA&A, 51, 105
Catinella, B., Schiminovich, D., Kauffmann, G., et al. 2012, A&A, 544, A65
Chabrier, G. 2003, PASP, 115, 763
Clemens, M. S., Negrello, M., De Zotti, G., et al. 2013, MNRAS, 433, 695
Combes, F., García-Burillo, S., Braine, J., et al. 2013, A&A, 550, A41
Daddi, E., Dickinson, M., Morrison, G., et al. 2007, ApJ, 670, 156
Donoso, E., Yan, L., Tsai, C., et al. 2012, ApJ, 748, 80
Fu, J., Kauffmann, G., Li, C., & Guo, Q. 2012, MNRAS, 424, 2701
Gao, Y., & Solomon, P. M. 2004, ApJ, 606, 271
Genzel, R., Tacconi, L. J., Gracia-Carpio, J., et al. 2010, MNRAS, 407, 2091
Giovanelli, R., Haynes, M. P., Kent, B. R., et al. 2005, AJ, 130, 2598
Guo, K., Zheng, X. Z., & Fu, H. 2013, ApJ, 778, 23
Haynes, M. P., Giovanelli, R., Martin, A. M., et al. 2011, AJ, 142, 170
Huang, S., Haynes, M. P., Giovanelli, R., & Brinchmann, J. 2012, ApJ, 756, 113
Kennicutt, R. C., & Evans, N. J. 2012, ARA&A, 50, 531
Kennicutt, Jr., R. C. 1998, ApJ, 498, 541
Kennicutt, Jr., R. C., Armus, L., Bendo, G., et al. 2003, PASP, 115, 928
Kennicutt, Jr., R. C., Hao, C.-N., Calzetti, D., et al. 2009, ApJ, 703, 1672
Krumholz, M. R. 2013, in IAU Symposium, Vol. 292, IAU Symposium, ed. T. Wong & J. Ott, 227–234
Leroy, A. K., Walter, F., Bigiel, F., et al. 2009, AJ, 137, 4670
Leroy, A. K., Walter, F., Sandstrom, K., et al. 2013, AJ, 146, 19
Lisenfeld, U., Espada, D., Verdes-Montenegro, L., et al. 2011, A&A, 534, A102
Rahman, N., Bolatto, A. D., Xue, R., et al. 2012, ApJ, 745, 183
Rodighiero, G., Daddi, E., Baronchelli, I., et al. 2011, ApJ, 739, L40
Saintonge, A., Kauffmann, G., Kramer, C., et al. 2011a, MNRAS, 415, 32
Saintonge, A., Kauffmann, G., Wang, J., et al. 2011b, MNRAS, 415, 61
Saintonge, A., Tacconi, L. J., Fabello, S., et al. 2012, ApJ, 758, 73
Sandstrom, K. M., Leroy, A. K., Walter, F., et al. 2013, ApJ, 777, 5
Schmidt, M. 1963, ApJ, 137, 758
Schruba, A., Leroy, A. K., Walter, F., et al. 2011, AJ, 142, 37
Solomon, P. M., Downes, D., Radford, S. J. E., & Barrett, J. W. 1997, ApJ, 478, 144
Spergel, D. N., Bean, R., Doré, O., et al. 2007, ApJS, 170, 377
Tacconi, L. J., Neri, R., Genzel, R., et al. 2013, ApJ, 768, 74
Walter, F., Brinks, E., de Blok, W. J. G., et al. 2008, AJ, 136, 2563
Wilson, C. D., Scoville, N., Madden, S. C., & Charmandaris, V. 2000, ApJ, 542, 120
Wright, E. L., Eisenhardt, P. R. M., Mainzer, A. K., et al. 2010, AJ, 140, 1868
Wyder, T. K., Martin, D. C., Schiminovich, D., et al. 2007, ApJS, 173, 293
Yan, L., Donoso, E., Tsai, C.-W., et al. 2013, AJ, 145, 55
Young, J. S., & Scoville, N. Z. 1991, ARA&A, 29, 581
Zhang, Z.-Y., Gao, Y., Henkel, C., et al. 2014, ApJ, 784, L31

APPENDIX

A. APERTURE EFFECT

Our study is affected by aperture effect from both the radio telescopes and *WISE*. On the one hand, the single dish telescopes (IRAM 30-m, FCRAO 14-m and SMT 10-m) mentioned above all have a finite aperture size (HPBW) and can only cover a portion of the CO emission from a galaxy observed if its angular size is significantly larger than the beam size of the dish. Thus for the majority of the sources, especially those observed with 30-m telescope whose HPBW was only 22″ at 115 GHz, an aperture correction from the observed CO flux to total CO flux was necessary. In the latest COLD GASS data release and the AMIGA sample, they both assume that the radial distribution of CO and molecular gas is exponential, and the CO scale length r_e correlates well with the optical radius at the 25mag isophote, $r_e = 0.2\ r_{25}$. Thus the correction from the observed CO flux to the total flux based on this model can be calculated. The technical details about the aperture correlation method can be found in Lisenfeld et al. (2011) and Saintonge et al. (2012).

On the other hand, the standard photometry pipeline of *WISE* adopted a series of circular apertures to measure the magnitudes of a galaxy, and the maximum aperture size used is 24.75″. Thus for some large galaxies their W3 will suffer from the same aperture issue, so the study of the relation between molecular gas and W3 relies on improved accurate photometry. However, since the angular sizes of the galaxies in our selected SMT sample is relatively suitable for both *WISE* and the SMT beam (33″ at 230 GHz) and could be effectively covered, we did not adopt this aperture correction for this sample, and Figure. 6b already shows a very robust correlation. There is a galaxy in Figure. 6b, whose $L_{12\,\mu\mathrm{m}}$ is about 9.4 $L_{\odot}$, showing deviation from the fitted line, and we confirmed that its enhanced $L_{12\,\mu\mathrm{m}}$ is due to the contamination from a nearby star, and the confusion could not be reduced because of the relatively large beam of *WISE*. Nevertheless this source does not affect the overall fitting results even it is included in the sample for statistics.

B. SMT CO 2-1 SPECTRA

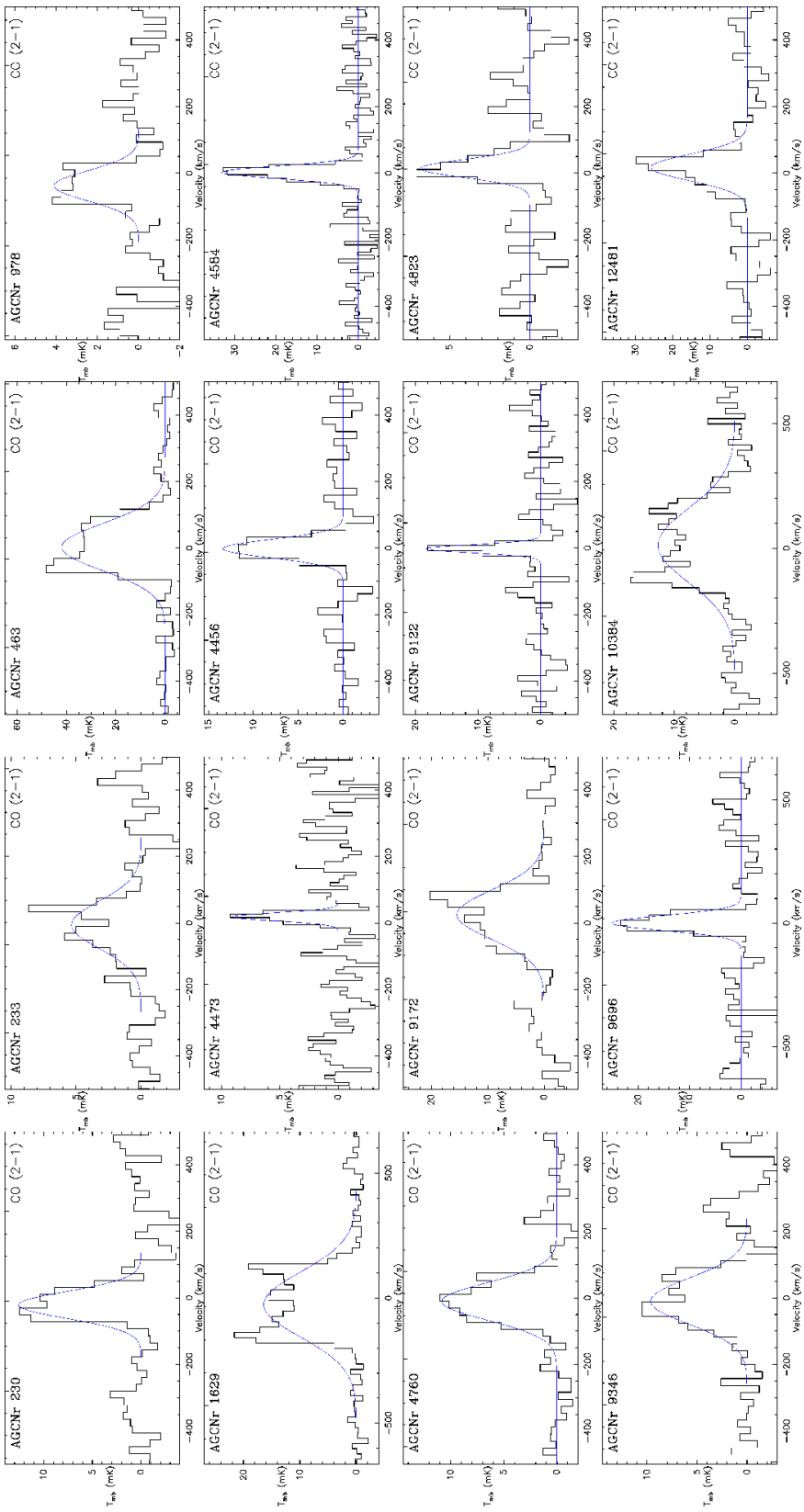

Figure 7. CO 2-1 spectra of the SMT sample (1). Source names from the ALFALFA are denoted in the upper left corner of each panel. The Gaussian profiles are only for reference but not used in the flux calculations.

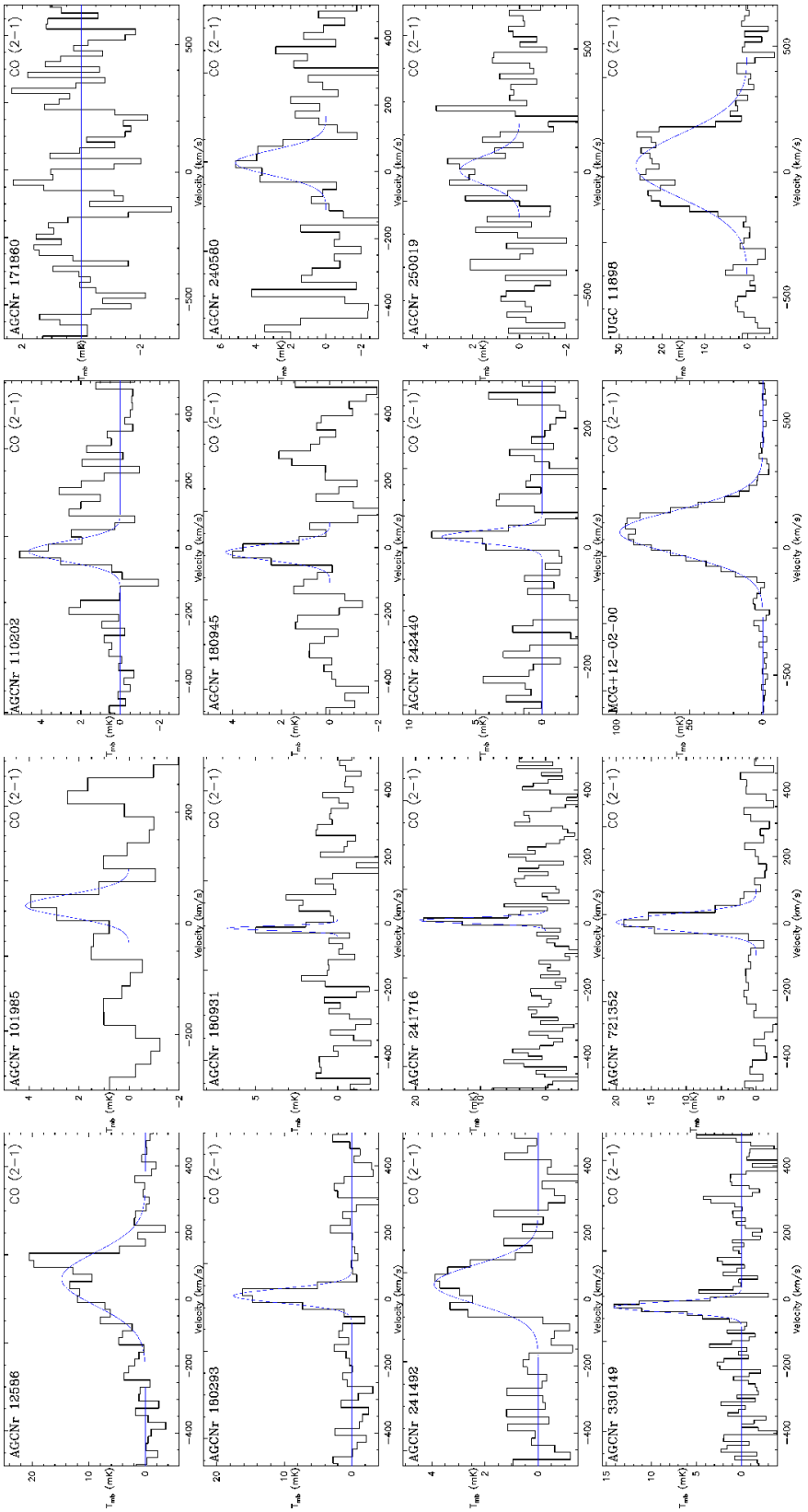

Figure 7. CO 2-1 spectra of the SMT sample (2). Source names from the ALFALFA are denoted in the upper left corner of each panel. The Gaussian profiles are only for reference but not used in the flux calculations.